GROUND DEFORMATION MONITORING OF RECLAIMED LANDS ALONG MANILA BAY FREEPORT ZONE USING PS-INSAR TECHNIQUE

A. L. Lomibao[1], G. A. Leal[1], L. C. Mabaquiao[1,2*], R. B. Reyes[1,2]

[1]Department of Geodetic Engineering, University of the Philippines – Diliman, Philippines –
(aalomibao, gsleal, lsmabaquiao, rbreyes3)@up.edu.ph

[2]Training Center for Applied Geodesy and Photogrammetry, University of the Philippines, Diliman, Quezon City

KEY WORDS: Interferometry, SARPROZ, Uplift, Subsidence, Disaster

ABSTRACT:

In response to escalating land demands, land reclamation plays a vital role, but this comes with the challenge of ground deformations that threaten livelihoods and safety. To address the growing concern, Persistent Scatterer Interferometric Synthetic Aperture Radar (PS-InSAR) is utilized. This remote sensing method is known for its cost-effectiveness, efficiency, and high-resolution capabilities, to monitor vertical ground deformations in Manila Bay Freeport Zone's reclaimed areas. Through adaptation and implementation of PS-InSAR via SARPROZ, measurements along the satellite's line-of-sight (LOS) is integrated both for ascending and descending geometries using the Nearest Neighbor Vector (NNV) approach to decompose and derive precise vertical displacement values. Correlation analysis with annual leveling data from six benchmarks reveals a strong relationship with correlation coefficient > 0.80. The results indicate relative stability with localized subsidence due to differential settlement and nearby construction. The results from the PS-InSAR technique show that ground deformation on reclaimed lands is expected to continue. Hence, monitoring should be implemented to observe sustained settlements after reclamation, identify areas with significant deformations, detect building and structural deformations, and initiate solutions to reduce the risk of environmental hazards.

1. BACKGROUND

1.1. Land Reclamation and Ground Deformation

Land reclamation is the process of improving or creating new lands from the sea to maximize its best use with the increasing demand for land. Reclamation can either be done by (1) draining submerged wetlands or by (2) raising the elevation of the ground by filling the area with soil and heavy rocks (Stauber et al., 2016). Reclamation projects hold a promising future for economic growth in the country, but they can adversely affect the environment. Land reclamation poses great risks of massive flooding due to sea level rise in the reclaimed area, which is also tied to the ground deformation in the form of subsidence or uplift. Ground deformation is a geological hazard that continuously disrupts economic and human activities throughout the world. It involves the sinking, rising, and/or shifting of the Earth's surface due to geological activities. Geological events like earthquakes, landslides, and volcanic eruptions can cause ground deformation (Erten & Rossi, 2019). Additionally, human actions like building construction, urban development, groundwater extraction, and land reclamation can also trigger deformation. This deformation damages properties and increases vulnerability to floods, ruptures, storm surges, and tidal impacts. As sea levels rise in the coming years, coastal residents face greater risks, intensifying the effects of ground deformation, especially in reclaimed lands (Syvitski et al., 2009).

Land subsidence is a type of deformation directed downward from the surface in the vertical direction (U-D movement) (Aboualy et al., 2021). Ground deformation in subsiding areas is caused by horizontal strains generated by localized differential compaction on the earth's fissures (Thomas, 2010). This deformation movement does not only account for the up-down direction but also the horizontal or planar direction. According to Sun et al. (2018), land subsidence has been a significant problem in reclaimed areas from the sea because of different settlement patterns caused by unconsolidated marine sediment and fill materials. The process of reclamation needs sustainable policies and development practices to prevent these risk factors that can affect people's livelihoods.

There are 175 proposed reclamation projects in the Philippines as of April 2022 (Philippine Reclamation Authority, 2022). Because of this, ground deformation in these areas continues to threaten the lives and livelihoods of the people by increasing their exposure to natural hazards, e.g., floods and storm surges. For this study, the researchers intend to introduce a satellite technique to monitor vertical ground deformations in the reclaimed lands in Manila Bay, particularly in the Manila Free Port Zone.

1.2. Ground Deformation Monitoring

Traditional geodetic techniques, such as direct leveling and the use of Global Navigation Satellite Systems, are frequently used for ground deformation detection (Li et al. 2022a). However, they are resource-intensive, requiring significant time and effort. The emergence of Interferometric Synthetic Aperture Radar (InSAR) technology has revolutionized this field, allowing ongoing and remote monitoring of deformations through the analysis of two or more Synthetic Aperture Radar (SAR) images stacked together. This satellite-based methodology enables wide scale ground monitoring covering extensive spatial extents. This method works irrespective of weather conditions, providing exceptional spatial and temporal detail. More importantly, InSAR excels in determining ground deformations within short time intervals (Hu et al., 2019).

SAR images are subjected to different incidence angles due to the Earth's curvature and rotation. The deformation measured using InSAR is projected in the Line of Sight (LOS) of the RADAR satellite. To determine the vertical component of the ground deformation, two separate RADAR tracks having different viewing geometry is necessary to decompose the vectors to the horizontal and vertical planes. Figures 1 and 2 show how both the ascending and descending paths of the satellite is utilized to derive the vertical component of the deformation. Despite the various applications of InSAR, the method introduces issues with decorrelation, phase unwrapping, and atmosphere biases due to

* Corresponding Author

the limitation of using only a pair of SAR images, limiting its potential (Perissin, 2016).

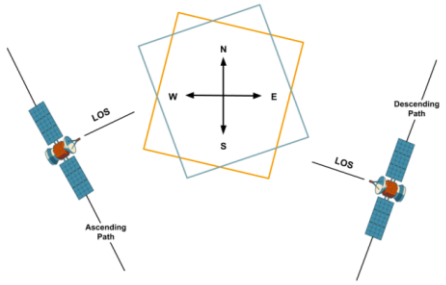

Figure 1. Orientation of ascending and descending satellite images (Vassileva et. al, 2017)

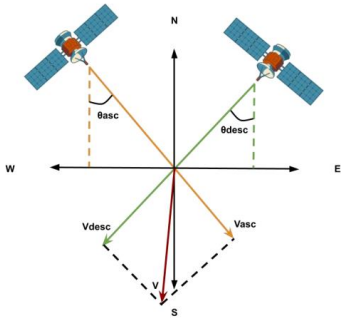

Figure 2. Observation geometries of satellite images in ascending and descending paths (Ding et. al. 2020)

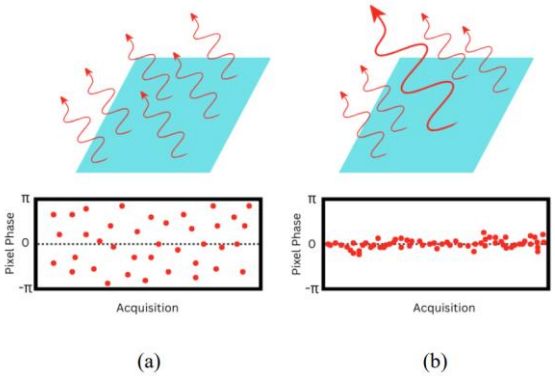

Figure 3. Phase simulation for a) distributed scatterer and b) persistent scatterer (Azeriansyah et al. 2019)

The MT-InSAR technique utilizes stacks of SAR images to overcome InSAR limitations. The most exploited MT-InSAR techniques are Small Baseline Subset (SBAS) and Persistent Scatterer (PS). Previous studies have proven that MT-InSAR has the capability to monitor ground deformations (Hussain et al., 2022). The validation of the MT-InSAR approach using in-ground measurements revealed good agreement between the observed deformation rates (Armaş et al., 2016)

The PS-InSAR approach, introduced by Ferretti et al. (2001), requires at least 20 images to generate reliable results. It is an opportunistic method wherein the analysis of measurements can only be performed in areas where PS points are detected. These points are characterized by the presence of a dominant backscatter per resolution cell over the acquisition period. This is seen in figure 3 where the presence of a dominant scatterer affects the ability of the MT-InSAR to perform long term analysis. The foundation of PS-InSAR depends on identifying persistent scatterer (PS) points based on the amplitude information (Jia & Liu, 2016). PS points are primarily located in stable areas, e.g., buildings, monuments, stones, and poles (Hu et al., 2019). The advantages of PS-InSAR are best appreciated when free available data, e.g., Envisat-ASAR and Sentinel-1, are used.

Studies assessing the application of the PS-InSAR in monitoring ground deformation on reclaimed areas have been undertaken during the last decade. Implementation of this method in urban areas situated on reclaimed lands yielded dense PS points. Some of these were identified as buildings. Significant deformation, i.e., subsidence, was observed in the reclaimed areas of Coastal Harbor Peninsula, South Korea, and Qianhai District, China. The findings may be attributed to the reclamation period when the images were acquired and the type of fill material used (Kim et al., 2007). Results from the PS-InSAR approach are consistent with those from traditional geodetic techniques (Hu et al., 2019).

1.3. Objectives and Significance

The study generally aims to introduce a satellite-based method of monitoring the vertical ground deformation on reclaimed lands in Manila Bay. This study also aims to identify spatiotemporal patterns in three (3) major islands of the Manila Bay Freeport Zone, often known as Bay City: Cultural Center of the Philippines and Financial Center Area (CCP-FCA Island), Central Business Park I-A (CBP I-A Island), and Central Business Park I-B & I-C (CBP IB & IC Island)

This study will help government agencies such as PRA and local government units (LGU) to monitor the surface behaviors of highly economic and highly-populated reclaimed areas. This study will also aid the people who reside in these reclaimed areas to be aware of the hazard and possibility of land subsidence in their region. Furthermore, the study hopes to initiate solutions to reduce the risks caused by land subsidence ang highlight the importance of consistent ground deformation monitoring in preventing economic or property losses. Lastly, monitoring deformations allows effective planning of future reclamation and sustainable development projects which is relevant to the upcoming projects approved by PRA.

2. MATERIALS AND METHODS

2.1. Study Area

Previously known as Bay City, Manila Bay Freeport Zone is a reclaimed land that can be found at 14° 31′ 25.14″ N and 120° 59′ 1.82″ E. Since it is Philippine Reclamation Authority's largest completed reclamation project, it was selected as the research study area. The issues considered also include the area's densely populated surroundings, which include substantial ground-level building loads, and its proximity to Manila Bay, which could result in flooding and subsidence because of tides and currents.

The general topography of Metro Manila is primarily flat along the coastal areas. Similarly, the study area is flat and is geographically located on the coastal margin facing Manila Bay, where the general climate features dry seasons (January-May), wet seasons (June-December), and intermittent tropical monsoons. Moreover, a geological map from Daag et al. (2022) shows that the reclaimed areas are geologically classified among the quaternary alluvium. It is mainly composed of unconsolidated materials such as detrital deposits, silt, sand, and gravel (MGB, 1983).

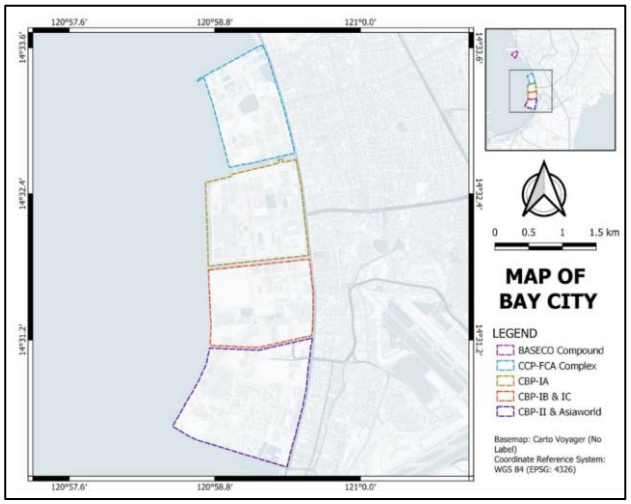

Figure 4. Map of Manila Bay Freeport Zone

Based on the interview conducted in PRA, the fill materials used for reclaiming CCP-FCA island came from mountain sources. On the other hand, the reclamation processes of Central Business Parks utilized European technology where dredging vessels were used to fill the area with sand. The stabilization process of the reclaimed land is composed of soil consolidation and soil compaction. A standard of 90% consolidation was enforced on all reclamation projects in PRA. The soil compaction method, on the other hand, varies from each section of the Manila Bay Freeport Zone.

2.2. Synthetic Aperture RADAR Images

To monitor the changes on the study area's surface, scenes were acquired from Sentinel 1 to cover the area of the Manila bay Freeport Zone. Both 1A and 1B SLC images were taken from 2018 to 2021. Temporal interval of 12 days was chosen in the Interferometric Wide (IW) mode. VV polarization was used since it backscatters a higher energy that results in a higher PS point detection in an urban area.

Sentinel-1 satellite images were used in this study because it has a complete set of satellite images in a 12-day interval from 2018-2021. According to Cian, et al. (2019), a larger density of PS points was detected using Sentinel-1 images in a particular area of interest. The PS points using Sentinel-1 have precise values because it has a relatively low standard deviation. However, the density of PS points depends on the land cover, resolution and the period the satellite images were acquired. A total of 119 SAR images for each ascending and descending was utilized.

DATA INFO	ASCENDING	DESCENDING
Satellite Mission	Sentinel 1-B	Sentinel 1-A
Number of scenes	119	119
Acquisition Period	Jan. 9, 2018 – Dec. 19, 2021	Jan. 7, 2018 - Dec 29, 2021
Path	142	32
Satellite Heading Angle	-168.9718	-11.0666
Central Heading Angle	39.3097	39.4182
Acquisition Time (UTC)	10:06	21:46
Band	C-band (5.65 cm wavelength)	
Revisit Period	12 days	
Range and Azimuth Spacing	3.67m x 14.00m	
Acquisition Mode	Interferometric Wide Swath (IW)	
Product Type	Single Look Complex (SLC)	
Polarization	VV	

Table 1. Details of SAR datasets used

2.3. Leveling Data

Benchmarks used for this study are situated within the Port Area. The annual levelling data of the benchmarks near the study area were obtained from NAMRIA. Table 2 shows the coordinates of each benchmark and its cumulative displacement values used for validating the PS-InSAR data.

BM	CUMULATIVE DISPLACEMENT (mm)					POSITION	
	2018	2019	2020	2021	2022	Latitude	Longitude
TGBMCG2	0	-2.00	-8.38	-5.56	-9.31	14°34'57.51"N	120°58'16.48"E
TGBM1	0	0.41	-5.56	-3.85	-4.72	14°35'1.52"N	120°58'21.44"E
TGBM3	0	-0.63	-6.82	-5.66	-5.95	14°35'15.44"N	120°58'10.58"E
BM66	0	-1.02	-7.58	-7.67	-12.03	14°35'10.62"N	120°58'4.33"E
BM32C	0	-2.29	-7.09	-5.70	-7.85	14°35'31.66"N	120°58'23.03"E
BM5	0	-3.93	-8.35	-6.11	-8.64	14°35'40.57"N	120°58'40.18"E

Table 2. Leveling Data of Benchmarks near the AOI.

2.4. General Methodology

The methodology of the study consists of the following parts: (1) PS-InSAR Processing, (2) vector-based approach for combining ascending and descending LOS data, (3) validation of the results, and (4) stability thresholding. PS-InSAR processing uses the stack of SAR images to select PS points in the study area to determine the surface's movement relative to the satellite's LOS. Then the derived LOS measurements were analyzed using statistical evaluation to decompose the vertical and horizontal components of the deformation vector.

The Nearest Neighbor Vector (NNV) approach was used to decompose vectors and dervie the vertical component of ground deformation. Thresholding is done to classify the detected PS points as uplifting or subsiding depending on the standard deviation value. This is done to better interpret which points are moving and are statistically significant. Leveling data of benchmarks were used to validate PS-InSAR results.

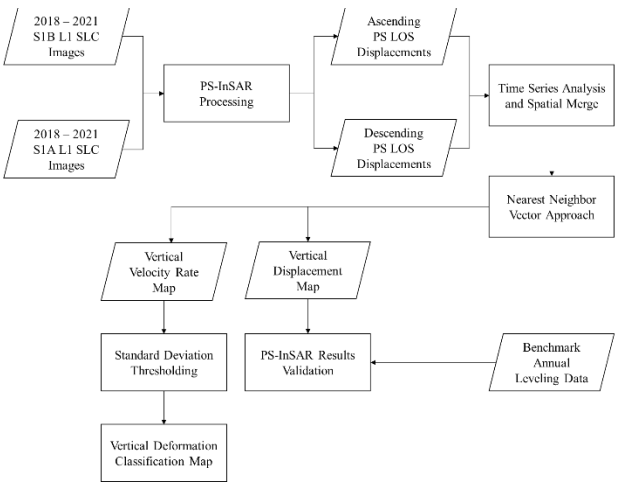

Figure 5. General workflow of the study

2.5. PS – InSAR Processing

The PS-InSAR algorithm is implemented using SARPROZ, a commercial software based on MATLAB (Qin & Perissin, 2015). Two stacks of images were processed independently for both sets of 1A and 1B. The stacks consist of 119 images acquired for each

geometry from January 2018 to December 2021. In this study, the PS-InSAR results were validated based on the annual vertical displacements measured for each benchmark. The master image was manually selected to ensure optimal perpendicular and temporal baselines. images dated February 4, 2020, and May 20, 2020, were used as the master images for the ascending and descending datasets, respectively. The perpendicular baselines of the slave images, with respect to the master image, are checked not to exceed the critical baseline value. The coregistration was done using precise orbits and the Copernicus DEM.

To identify the PS candidates, SARPROZ calculates the Amplitude Stability Index (ASI) using the amplitude values from the reflectivity map.

$$ASI = 1 - D_A = 1 - \frac{\sigma_A}{m_A} \quad (1)$$

where D_A is the dispersion index, the measure of phase stability, σ_A and m_A represents the standard deviation and the mean of the amplitude values, respectively. Absolute amplitude values are not much affected by phase contributors. Thus, small phase dispersion is expected from pixels exhibiting similar amplitude values throughout the acquisition (Fárová et al., 2019)

Ferretti et al. (2001) proposed selecting PS based on the threshold set for amplitude values: ASI > 0.75. For this study, a stricter standard for selecting PS was implemented to improve the accuracy of APS estimation. The threshold for both ascending and descending stacks were set to ASI > 0.80. The ASI criterion was chosen as a compromise between the quality of the points and the spatial coverage (Beladam et al., 2019). These points were connected using the Delaunay triangulation to establish a reference network. The initial parameters were estimated using these connections. These parameters were then integrated using a reference point to calculate the absolute values for each PS candidates. Both reference points are located away from areas with known deformations and near each other to reduce the contamination of the velocity rates due to their location. APS was estimated from the phase residuals by graph inversion after removing the previously estimated linear model, which was based on the linear deformation rates and the residual height (Fárová et al., 2019). Afterwards, the estimated APS was removed from the results.

Subsequent estimation of the parameters for a new set of points was performed for the Multi-Image Sparse Point Processing stage. A less stringent criterion was adopted in the second PS selection. Relaxing the criterion resulted in denser PS points. The parameters used for estimating linear trend and height were adjusted based on the resulting ranges of the integrated velocity and residual height (Qin, 2018). The final processing was executed using the same reference point from the previous stage. The PS points were then exported and geocoded. Additionally, the derived time series data for each point were obtained. PS points with high temporal coherence, greater than 0.70, were used to analyze the PS-InSAR technique results. Further processing of the PS-InSAR results was performed in QGIS.

The acquisition and processing of PS-InSAR data aims to determine the vertical (U-D) component of ground deformation in reclaimed areas derived from the resulting velocities of the Sentinel-1 ascending and descending LOS geometries. In this study, the vertical component of deformation was derived using a vector-based approach for integrating ascending and descending PS points measurement.

The NNV approach was implemented to determine the closest PS point from the opposing geometry. Subsequent analysis concerning the decomposition of the vertical component of deformation was then limited to a maximum radius of 50 m, about thrice the median value of the distance between PS points.

2.6. Validation using Leveling Data

To evaluate the consistency of the PS-InSAR results with the ground truth data, the vertical displacement of the selected PS point will be correlated with the leveling data. The strength of the relationship of the result was determined using the classification in Table 3 as used by De Lara et al. (2022).

CORRELATION VALUE (r)	DESCRIPTION
1	Perfect
0.7 - 0.9	Strong
0.4 - 0. 6	Moderate
Less than 0.3	Weak

Table 3. Description of correlation values De Lara et al. (2022)

2.7. Standard Deviation and Thresholding

The values were classified into three categories using standard deviation thresholding, as seen in Table 4. Each classification's upper and lower limit was determined by converting the values into standard deviation intervals (Fárová et al., 2019). In order to identify the intervals, the mean and standard deviation of the vertical velocity rate of the PS points in the processed area were calculated. The stability threshold of the result is equal to 1.5 times the standard deviation values.

CLASSIFICATION	Standard Deviation Interval
Uplift	> +1.5 Std. Dev
Stable	+1.5 Std. Dev – -1.5 Std. Dev
Subsidence	< -1.5 Std. Dev

Table 4. Standard deviation intervals for the classification of vertical deformation

3. RESULTS AND DISCUSSION

STUDY AREA	Ascending (Path 142)		Descending (Path 32)	
	NO. OF PS	DENSITY (PSs/km^2)	NO. OF PS	DENSITY (PSs/km^2)
Bay City				
CCP-FCA Complex	455	289	418	266
CBP-IA	754	380	940	474
CBP-IB & IC	339	186	403	221
CBP-2 & Asiaworld	498	189	491	186

Table 5. Distribution of PS points in the study area

Results reveals that PS points are common on buildings, residences, exposed rocks, and permanent constructions. The area processed for the ascending track yielded a density of 489 PS/km^2, totaling 75,384 PS points. On the other hand, the area processed for the descending track produced a density of 504 PSs/km^2, with a total of 77,663 PS points. High-density PS detection in the processed area for both tracks affirm the

suitability of the PS-InSAR technique in monitoring deformations of urban areas.

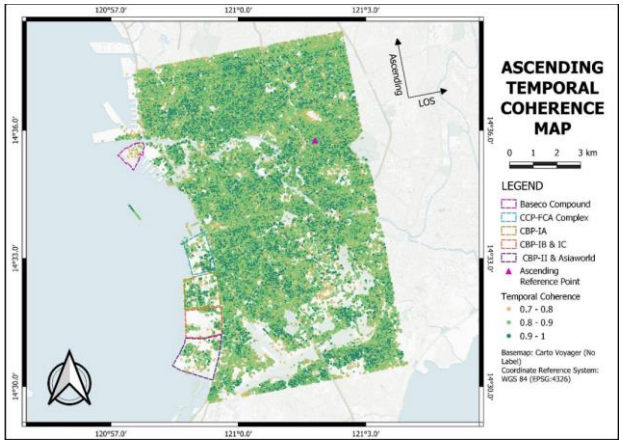

Figure 6. PS Point Distribution and Temporal Coherence Map for Ascending Track

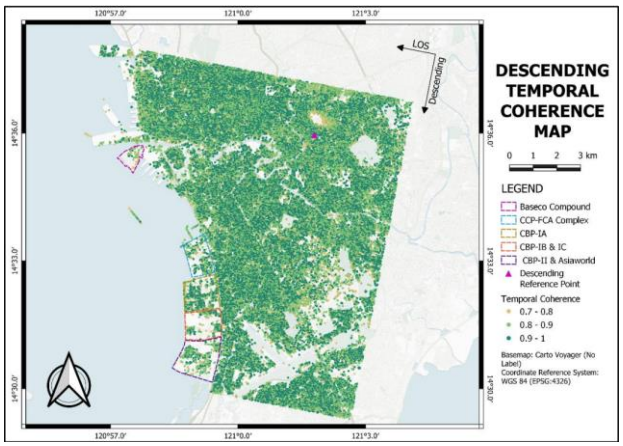

Figure 7. PS Point Distribution and Temporal Coherence Map for Descending Track

A pair of PS point from the ascending and descending tracks were selected for the analysis of the time series graph. These points are located on the same location where large LOS motions for each reclaimed islands are observed. Strong linearity in the time-series graphs is visible for all PS points in the ascending and descending time series as seen in figures 8 and 9. The R^2 value was identified for each point to determine its fitness with the linear model. All points in the ascending and descending track yielded an R^2 value greater than 0.85, hence giving confidence to the assumption of a linear deformation pattern in the study areas. PS points experience constant rate of deformation in the LOS direction.

Vertical motion of the deformation is derived by decomposing and merging the ascending and descending PS points. This results in denser PS, which is advantageous in analyzing deformations (Foumelis, 2018). Classification of PS points were done through standard deviation thresholding to determine stable, uplifting and subsiding points.

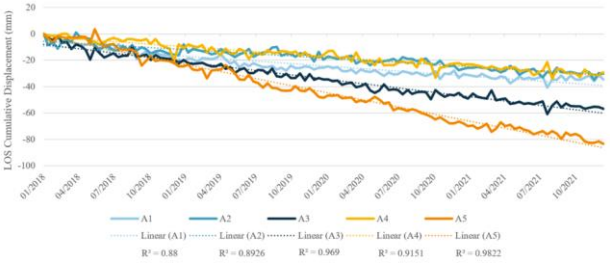

Figure 8. Ascending time series graph

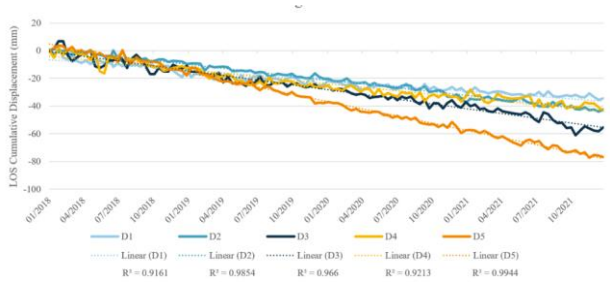

Figure 9. Descending time series graph

Each PS point was classified as uplift, stable, and subsidence using standard deviation thresholding. Table 6 shows the threshold values used for the classification.

Classification	Standard Deviation	Upper Limit	Lower Limit
Uplift	> 1.5 St. Dev.	—	2.20 mm/yr
Stable	1.5 to -1.5 St. Dev.	2.20 mm/yr	-6.32 mm/yr
Subsidence	< -1.5 St. Dev.	-6.32 mm/yr	—

Table 6. Upper and lower limit used for the thresholding of the vertical velocity rates (mm/yr)

After establishing the limits for each category, the map of vertical deformation was generated to visualize the clustering of subsiding and uplifting PS points

3.1. CCP – FCA Complex

For the CCP – FCA complex, a total of 20 PS points were classified as subsiding. These points are in two areas within the reclaimed island as shown in figure 10. The researchers were able to inspect the Seascape Village for signs of deformation since a cluster of subsiding points is found in the area. Subsiding points near the PSA outlet were isolated and surrounded by stable PS points, hence the area is relatively stable. Table 7 show the statistics of PS points within the CCP – FCA Complex

Total number of PS points within the area	817 points
Number of Subsiding Points	20 points
Average Vertical Cumulative Displacement	-2.90 ± 7.20 mm
Average Vertical Velocity Rate	-0.73 ± 1.82 mm/yr
Highest Velocity Rate	3.16 mm/yr
Lowest Velocity Rate	-9.86 mm/yr

Table 7. Statistics of PS points within CCP-FCA Complex

Seascape Village experiences the largest subsidence rate throughout the extent of CCP-FCA Island with an average rate of -8.22mm/year. However, various PS points in the northern part of the village were classified as stable regardless of their proximity to the edge of Manila Bay.

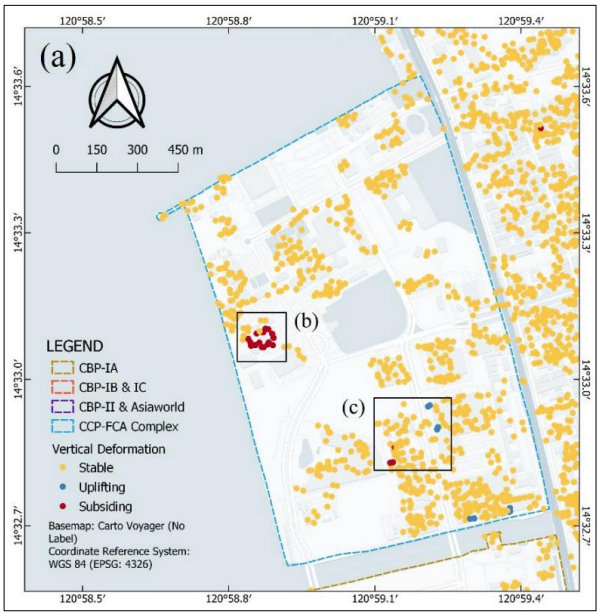

Figure 10. Vertical Deformation of CCP-FCA, (b) Seascape Village, and (c) PSA – Pasay outlet

The hypothesized cause of localized deformation in this area was further analysed based on the construction of nearby buildings as shown in figure 11. Dong et al. (2014) discussed that the construction of buildings induces differential subsidence in the area at a local scale. Upon closer inspection, it was discovered that the southernmost section of the recently built region is comprised of high-rise buildings situated roughly 50 meters away from Seascape Village. This can be attributed to the detected localized subsidence in the nearby area.

Figure 11. Historical satellite imagery of Seascape Village (5/2018 to 5/2020). Red dots indicate subsiding areas

3.2. CBP – IA

Majority of the areas in CBP-IA are classified as stable, as seen in Figure 12; however, subsiding points were found in the southwest area of the island. An average subsidence rate of 9.69 mm/yr was observed in that area. Table 8 contains the details of the deformations in the reclaimed island.

Cracks on cemented structures, sidewalks, and restaurant walls were seen in the area where a cluster of subsiding points is located. Generally, the whole island of CBP-IA was classified as stable except in this area.

Table 8. Statistics of PS points within CBP-IA

Total number of PS points within the area	1,634 points
Number of Subsiding Points	31 points
Average Vertical Cumulative Displacement	-6.40 ± 6.50 mm
Average Vertical Velocity Rate	-1.61 ± 1.64 mm/yr
Highest Velocity Rate	1.97 mm/yr
Lowest Velocity Rate	-13.35 mm/yr

Possible causes of subsidence may be associated with the settlement of loose sediments and compression of unconsolidated materials (Li et al. 2022).

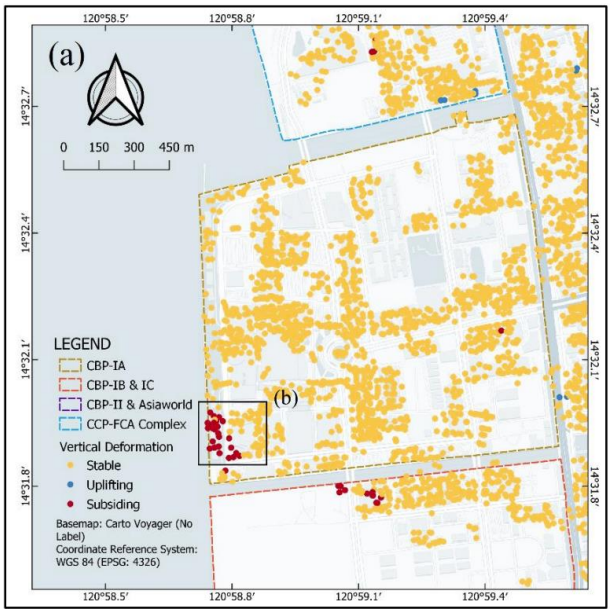

Figure 12. Classification map of vertical deformation of a) CBP – IA Island, and b) southern part of SM by the Bay

3.3. CBP-IB & IC

The CBP-IB & IC has 35 subsiding points out of 690 PS points. Based on Figure 13, there are three regions in the reclaimed area where there are concentrations of subsiding points present. Statistics of the PS points in the CBP-IB & IC island is shown in Table 9.

Total number of PS points within the area	690 points
Number of Subsiding Points	35 points
Average Vertical Cumulative Displacement	-10.02 ± 9.18 mm
Average Vertical Velocity Rate	-2.53 ± 2.32 mm/yr
Highest Velocity Rate	0.60 mm/yr
Lowest Velocity Rate	-17.60 mm/yr

Table 9. Statistics of PS points within CBP-IB & IC

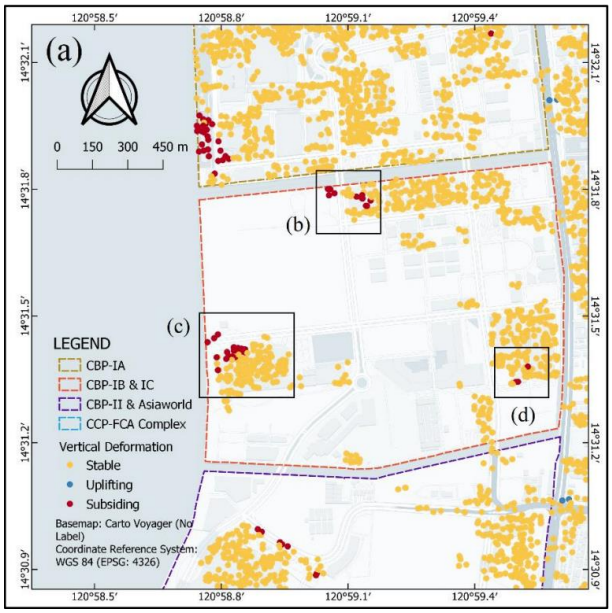

Figure 13. Classification map of vertical deformation of a) CBP-IB & IC Island, and b) Caltex Station, c) Solaire Resort, and d) near City of Dreams.

A total of 4 subsiding points around Caltex station were detected with the lowest velocity rate of -17.52 mm/yr. It is important to note that the road adjacent to the store is unpaved. Unpaved roads are susceptible to deformation (Palmeira & Cunha, 1993). This kind of road is also prone to erosion by wind or water which can lead to further deformation. Similarly, a few cracks and gaps were observed on each side of the bridge across the station.

3.1. Field Validation using Leveling Data

Benchmarks near the port of Manila area was used to validate the results of the PS-InSAR. Elevations of the benchmarks were referred to the zero-tide staff, with a vertical accuracy for 2nd-order leveling surveys. The leveling was conducted at the beginning of each year. The accumulated displacement of the PS points and the benchmarks show that the subsidence trend computed by the two methods is similar in terms of correlation coefficient. Figure 14 show the time series of the cumulative vertical displacements of the PS points found nearest for each benchmark. Both PS-InSAR and leveling data have a subsiding trend in the area. The PS-InSAR acquired larger vertical velocity rates, resulting in larger estimated vertical displacements compared to the displacements from the leveling data. An increased in January 2021 leveling reading was observed for majority of the benchmarks.

Annual leveling data and PS-InSAR results have a strong positive linear relationship based on the classification of the correlation values. De Lara et al. (2022) state that a high correlation reinforces the PS-InSAR result's reliability. Thus, PS-InSAR is capable of identifying areas experiencing vertical deformations in the absence of conventional geodetic techniques.

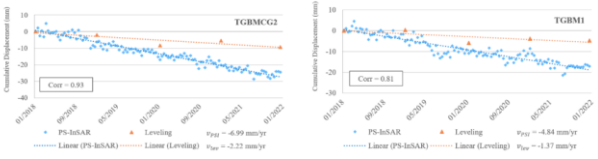

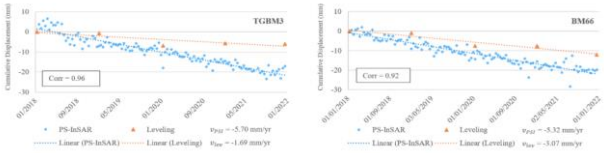

Figure 14. Time Series Graph of Cumulative Displacement in Benchmarks in Manila

the accumulated displacement of the PS points and the benchmarks show that the subsidence trend computed by the two methods is similar with the correlation value ranging from 0.81 to 0.96. This shows that the PS-InSAR results are reliable for vertical displacement measurements.

4. CONCLUSIONS

This research utilized 119 Sentinel-1 SAR images for each ascending and descending track to monitor the ground deformation of reclaimed lands along manila bay from 2018-2021. Ascending and descending LOS measurements exhibit a linear pattern of deformation. Vertical displacements were derived by decomposing the ascending and the descending LOS. The mean vertical velocity rate in the processed area is -2.06 ± 2.84 mm/yr. Assessment of the results of this study was done by comparing the vertical displacements obtained from the leveling data and PS-InSAR results. The cumulative displacement for each benchmark and PS point yielded high correlation values greater than 0.80. This indicates a strong linear relationship which gives a higher confidence in the results.

Aside from the leveling data, field inspection also confirmed the subsidence or settlements in the study area. Evidence of cracks and gaps was seen near the subsiding PS point locations. In addition, the same evidence can also be associated with exposure of risk to environmental hazards. Studies suggest that subsidence in the area increases the exposure to coastal hazards such as flooding and storm surges (Eco et al., 2020)

Majority of the Manila Freeport Zone contain stable PS points throughout each island. Several subsiding PS points were detected in the study area. These area are subjected to localized deformations since the reclamation islands are relatively stable. Average velocity rates of -0.73 ± 1.82 mm/yr, -1.61 ± 1.64 mm/yr, -2.53 ± 2.32 mm/yr, and -2.74 ± 1.86 mm/yr were observed among CCP-FCA, CBP-IA, CBP-IB & IC, and CBP-II & Asiaworld, respectively.

Overall, the PS-InSAR technique can successfully identify localized deformation and subsidence on reclaimed lands without prior knowledge of the deformation in the area. This technique is also helpful in detecting building and structure deformation since PS-InSAR is susceptible to detecting PS points in urban areas, locating areas suffering from a potential risk of subsidence, identifying areas experiencing significant deformations, and monitoring sustained settlements at millimeter level on reclaimed areas through time.

REFERENCES:

Armaş, I. et.al. 2016. InSAR Validation Based on GNSS Measurements in Bucharest. International Journal of Remote Sensing, 37(23), 5565–5580.

Azeriansyah, R. et. al. 2019. Land Subsidence Monitoring in Semarang and Demak Coastal Areas 2016-2017 Using Persistent

Scatterer Interferometric Synthetic Aperture Radar. IOP Conference Series, 313, 012040.

Abou Aly, N. et. al. 2021. Land deformation monitoring by GNSS in the Nile Delta and the measurements analysis. Arabian Journal of Geosciences, 14(3).

Cian, F. et. al. 2019. Sentinel-1 for Monitoring Land Subsidence of Coastal Cities in Africa Using PSInSAR: A Methodology Based on the Integration of SNAP and StaMPS. Geosciences, 9(3), 124.

De Lara, P. et. al. 2022. Estimation of Net Absolute Sea Level Change in Mogpog, Marinduque using Persistent Scatterer Interferometric Synthetic Aperture Radar-derived Vertical Land Motion and Tide Gauge

Ding, J. et. al. 2020. On the Characterization and Forecasting of Ground Displacements of Ocean Reclaimed Lands. Remote Sensing, 12(18), 2971.

Dong, S. et. al. 2014. Time-series analysis of subsidence associated with rapid urbanization in Shanghai, China measured with SBAS InSAR method. Environmental Earth Sciences, 72(3), 677–691.

Eco R.C. et. al. 2020. Disaster in Slow Motion: Widespread Land Subsidence in and Around Metro Manila, Philippines Quantified By InSAR Time-Series Analysis. JSM Environ Sci Ecol 8(1): 1068.

Erten, E. and Rossi, C. 2019. The worsening impacts of land reclamation assessed with Sentinel-1: The Rize (Turkey) test case. International Journal of Applied Earth
Observation and Geoinformation, 74, 57–64.

Fárová, K. et. al. 2019. Comparing DInSAR and PSI Techniques Employed to Sentinel-1 Data to Monitor Highway Stability: A Case Study of a Massive Dobkovičky Landslide, Czech Republic. Remote Sensing, 11(22), 2670.

Ferretti, A. 2001. Permanent Scatterers in SAR interferometry. IEEE Transactions on Geoscience and Remote Sensing, 39(1), 8–20.

Foumelis, M. 2018. Vector-based approach for combining ascending and descending persistent scatterers interferometric point measurements. Geocarto International, 33(1), 38–52.

Hu, B. et. al. 2019. Monitoring the Land Subsidence Area in a Coastal Urban Area with InSAR and GNSS. Sensors, 19(14), 3181.

Li, G. et. al. 2022. Land Subsidence Monitoring and Dynamic Prediction of Reclaimed Islands with Multi-Temporal InSAR Techniques in Xiamen and Zhangzhou Cities, China. Remote Sensing, 14(12), 2930.

Palmeira, E. M. and Cunha, M. P. 1993. A study of the mechanics of unpaved roads with reference to the effects of surface maintenance. Geotextiles and Geomembranes, 12(2), 109–131.

Perissin, D. 2016. Interferometric SAR Multitemporal Processing: Techniques and Applications. Multitemporal Remote Sensing, pp. 145–176.

Philippine Reclamation Authority. 2022. Proposed Reclamation Project in the Philippines. In FOI Philippines.

Qin, Y. and Perissin, D. 2015. Monitoring Ground Subsidence in Hong Kong via Spaceborne Radar: Experiments and Validation. Remote Sensing, 7(8), 10715–10736.

Ramirez, R. et. al. 2022. Monitoring of construction-induced urban ground deformations using Sentinel-1 PS-InSAR: The case study of Tunneling in Dangjin, Korea. International Journal of Applied Earth Observation and Geoinformation, 108, 102721.

Sany, S. et. al. 2019. The West Coast of Peninsular Malaysia. World Seas: An Environmental Evaluation, 437–458.

Sun, Q. et. al. 2018. Monitoring Coastal Reclamation Subsidence in Hong Kong with Distributed Scatterer Interferometry. Remote Sensing, 10(11), 1738. https://doi.org/10.3390/rs10111738

Stauber, J. et. al. 2016. Global Change. Marine Ecotoxicology, 273–313.

Syvitski, J, et. al. 2009. Sinking deltas due to human activities. Nature Gecience, 2(10), 681–686.

Thomas, H. 2010. Implications Of Ground-Deformation Measurements Across Earth Differential Settlements - Causes, Methods Of Prevention And Remediation. Geotech. https://www.geotech.hr/en/differential-settlements/

Vassileva, M. et. al. 2017. Satellite SAR interferometric techniques in support of emergency mapping. European Journal of Remote Sensing, 50(1), 464–477.